Journal of Structural Geology 31 (2009) 512–522

Contents lists available at ScienceDirect

Journal of Structural Geology

journal homepage: www.elsevier.com/locate/jsg

Reliability of magnetic fabric of weakly deformed mudrocks as a palaeostress indicator in compressive settings

Ruth Soto [a,*], Juan C. Larrasoaña [a], Luis E. Arlegui [b], Elisabet Beamud [c], Belén Oliva-Urcia [b], José L. Simón [b]

[a] Instituto de Ciencias de la Tierra "Jaume Almera", CSIC, C/Solé Sabarís s/n, 08028 Barcelona, Spain
[b] Departamento de Ciencias de la Tierra, Universidad de Zaragoza, Pedro Cerbuna 12, 50009 Zaragoza, Spain
[c] Laboratorio de Paleomagnetismo UB-CSIC, C/Solé Sabarís s/n, 08028 Barcelona, Spain

ARTICLE INFO

Article history:
Received 14 October 2008
Received in revised form
2 March 2009
Accepted 10 March 2009
Available online 24 March 2009

Keywords:
Anisotropy of magnetic susceptibility (AMS)
Palaeostress analyses
Mudrocks
Mesostructures
Ebro basin

ABSTRACT

In this work we compare the results of anisotropy of magnetic susceptibility (AMS) with palaeostress analysis at local scale. The AMS data refer to 14 sites from weakly deformed mudrocks (Lower and Middle Miocene lacustrine sediments) from two areas of the internal part of the Ebro foreland basin, the Bardenas Reales and Monegros areas. Nine sites display a magnetic fabric related to a subtle tectonic overprint showing a roughly E–W magnetic lineation, whereas the rest of sites (most of them located at the Monegros area) show a sedimentary fabric without a well-defined magnetic lineation. Palaeostress data result from fault populations and joint sets exposed in the limestone beds interbedded with the mudrocks at the nearest possible outcrop from the AMS site. The origin of the magnetic lineation is related to a N–S compression coeval with the earliest diagenesis of the studied sediments prior to consolidation. The comparison between magnetic fabric and palaeostress data demonstrates the coaxiality between the AMS and palaeostress ellipsoids both at local and regional scales, thereby validating the reliability of AMS as palaeostress indicator in compressive settings.

1. Introduction

The anisotropy of magnetic susceptibility (AMS) is a fast and non-destructive technique that has gained the acceptance of earth scientists because it allows characterizing even very subtle rock fabrics and provides valuable information on the origin and subsequent deformational history of rocks (e.g. Tarling and Hrouda, 1993; Borradaile and Henry, 1997). Of particular interest for structural geologists is the study of the AMS of weakly deformed mudrocks, since it records the initial stages of deformation both in compressive (Kissel et al., 1986; Mattei et al., 1997; Sagnotti et al., 1998, 1999; Parés et al., 1999; Larrasoaña et al., 2004; Cifelli et al., 2004a) and extensional settings (Mattei et al., 1997, 1999; Sagnotti et al., 1994; Cifelli et al., 2004a,b, 2005; Borradaile and Hamilton, 2004). We refer to weakly deformed mudrocks as these very fine-grained, clay-rich rocks (e.g. mudstones, claystones and siltstones) are either flat-lying or gently tilted or faulted and do not show any fabric apart from that related to deposition and compaction (see Parés, 2004). Following this definition, weakly deformed mudrocks include the so-called "undeformed" clays of Kissel et al. (1986) and Cifelli et al. (2004b, 2005). In the last years, the AMS of weakly deformed mudrocks has experienced a renewed interest since a growing body of evidence suggests that their magnetic fabric is locked-in during the earliest diagenesis, when the mudrocks are still unconsolidated, flat-lying, and the presence of water allows particulate flow by intergranular slip and kinking (Parés et al., 1999; Larrasoaña et al., 2004). During this incipient deformation, even in very low strain conditions, tectonic deformation is able to overcome the initial sedimentary fabric and to reorient phyllosilicate grains according to the prevailing stress field (Richter et al., 1993; Benn, 1994). Such reorientation results in development of a magnetic lineation which is perpendicular to the shortening direction in compressive settings (Kissel et al., 1986; Mattei et al., 1997; Sagnotti et al., 1998, 1999; Parés et al., 1999; Parés and van der Pluijm, 2002; Parés, 2004; Larrasoaña et al., 2004) and parallel to the stretching direction in extensional contexts (Mattei et al., 1997, 1999; Sagnotti et al., 1994; Cifelli et al., 2004a,b, 2005; Borradaile and Hamilton, 2004; Soto et al., 2007). Based on this, magnetic fabric has been considered as reliable indicators of palaeostress directions, which is important because mudrocks are ubiquitous in most tectonic settings, and the study of their magnetic fabric might provide new palaeostress results from structural units that very often lack strain markers and lithologies prone to be studied by

* Corresponding author. Present address: Dpto. Geodinámica y Geofísica, Facultad de Geología, Universidad de Barcelona, C/Martí Franquès s/n, 08028 Barcelona, Spain. Tel.: +34 934035957.
E-mail address: rsoto@ub.edu (R. Soto).

0191-8141/$ – see front matter © 2009 Elsevier Ltd. All rights reserved.
doi:10.1016/j.jsg.2009.03.006

standard palaeostress methods (e.g. fault and joint populations). Despite the potential of magnetic fabric as palaeostress indicators in weakly deformed mudrocks, there are few cases where the reliability of such magnetic fabric has been contrasted against palaeostress results (Kissel et al., 1986; Lee et al., 1990; Sagnotti et al., 1994, 1999; Mattei et al., 1997, 1999; Borradaile and Hamilton, 2004; Cifelli et al., 2004a, 2005; Soto et al., 2007).

In this paper, we present new AMS results from weakly deformed mudrocks that crop out in two sectors (Bardenas Reales and Monegros areas, Fig. 1) from the central part of the Ebro foreland basin (northern Spain). These results are combined with previously published (Arlegui and Simón, 1998, 2001; Simón et al., 1999), unpublished and new palaeostress data obtained from fault populations and joint sets developed on limestone beds interbedded with the mudrocks. Systematic comparison of AMS and palaeostress results, both at local and regional scales, provides a detailed evaluation of the origin and significance of the magnetic fabric in the studied mudrocks. The knowledge of the evolution of the Neogene stress field in the Ebro basin within the geodynamic scenario of the northeastern Iberian Peninsula (see Arlegui, 1996) makes the Ebro basin an ideal location to contrast the reliability of magnetic fabric as palaeostress indicator.

2. Geological setting

2.1. The Ebro foreland basin

The Ebro basin is a triangular-shaped basin that formed during the Tertiary at the foreland of the Pyrenees, the Iberian, and the Catalan Coastal ranges fold-and-thrust belts (Alonso-Zarza et al., 2002) (Fig. 1). Tectonic uplift occurred in the latest Eocene in the western Pyrenees and the Catalan Coastal Ranges cut the connection of the Ebro basin with the open ocean (Alonso-Zarza et al., 2002). The Ebro basin subsequently developed as an internally drained depression until the Late Miocene (Alonso-Zarza et al., 2002), when the Mediterranean drainage network captured the basin (García-Castellanos et al., 2003). The Ebro basin comprises a continuous sequence of latest Eocene, Oligocene and Miocene continental sediments (Alonso-Zarza et al., 2002). Thick conglomerate sequences deposited at the margins of the basin record the main tectonic events in the Pyrenees, the Iberian, and the Coastal Catalan ranges. Toward the central part of the basin, conglomerates grade to sandstones and mudstones of alluvial and fluvial origin. Such fluvial systems converged into the internal sector of the basin, where palustrine areas and extensive freshwater and saline lake systems developed depending on climate conditions. The stratigraphic sequence reaches more than 5500 and up to 3000 m in thickness in the Pyrenean (north) and Iberian (south) margins, respectively (Alonso-Zarza et al., 2002). Such difference between the northern and southern margins of the basin attests for the flexural subsidence of the foreland basin in response to tectonic loading by the Pyrenean allochtonous units (Muñoz, 1992).

2.2. Brittle mesostructures and palaeostresses in the Neogene Ebro basin

Continental sediments of the central part of the Ebro basin are affected by different fracture systems at the outcrop scale that include several joint sets as well as reverse, strike-slip and normal faults (Fig. 2) (Arlegui and Simón, 1998, 2001; Simón et al., 1999). These structures are especially well exposed in the lacustrine sediments that crop out at the Bardenas Reales and Monegros areas, where the presence of limestones favoured development of fractures, with preservation of kinematic indicators on their surface. The excellent exposure conditions allow determination of the geometry and timing relationships between different fracture systems, which developed according to the following general sequence: 1) E–W striking reverse faults; 2) NNW to NNE striking strike-slip faults; 3) N–S striking joints; 4) N to NE striking normal faults; and 5) E–W striking joints. E–W striking reverse and NNW to NNE striking

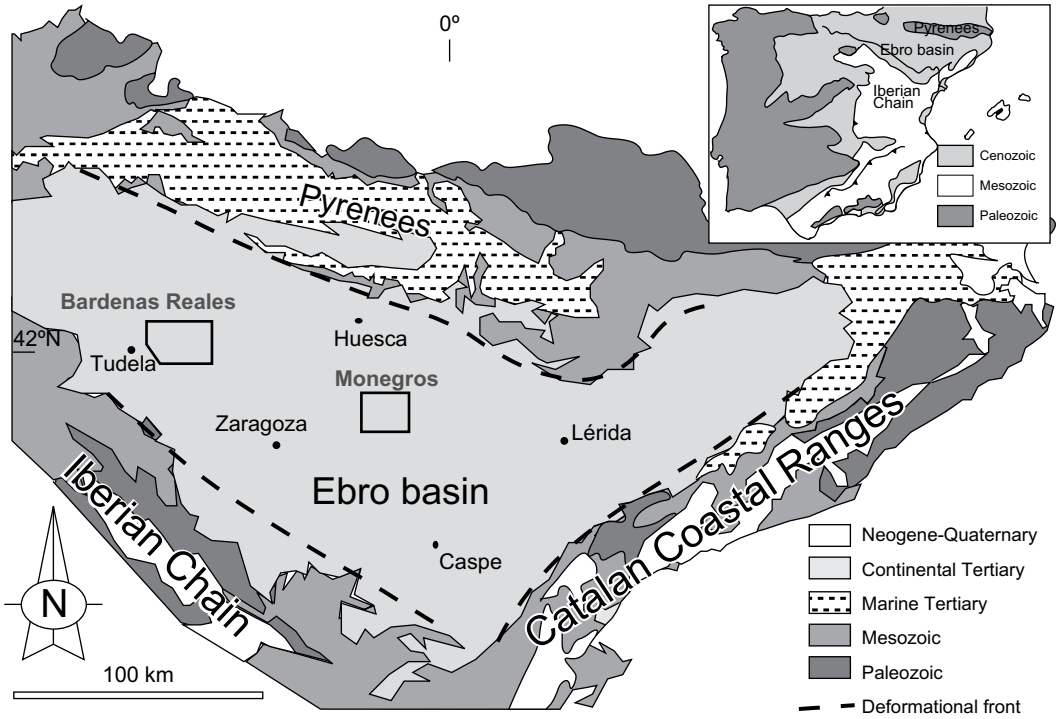

Fig. 1. Geological sketch map of the Ebro basin, with location of the Bardenas Reales and Monegros areas shown in Figs. 3 and 4.

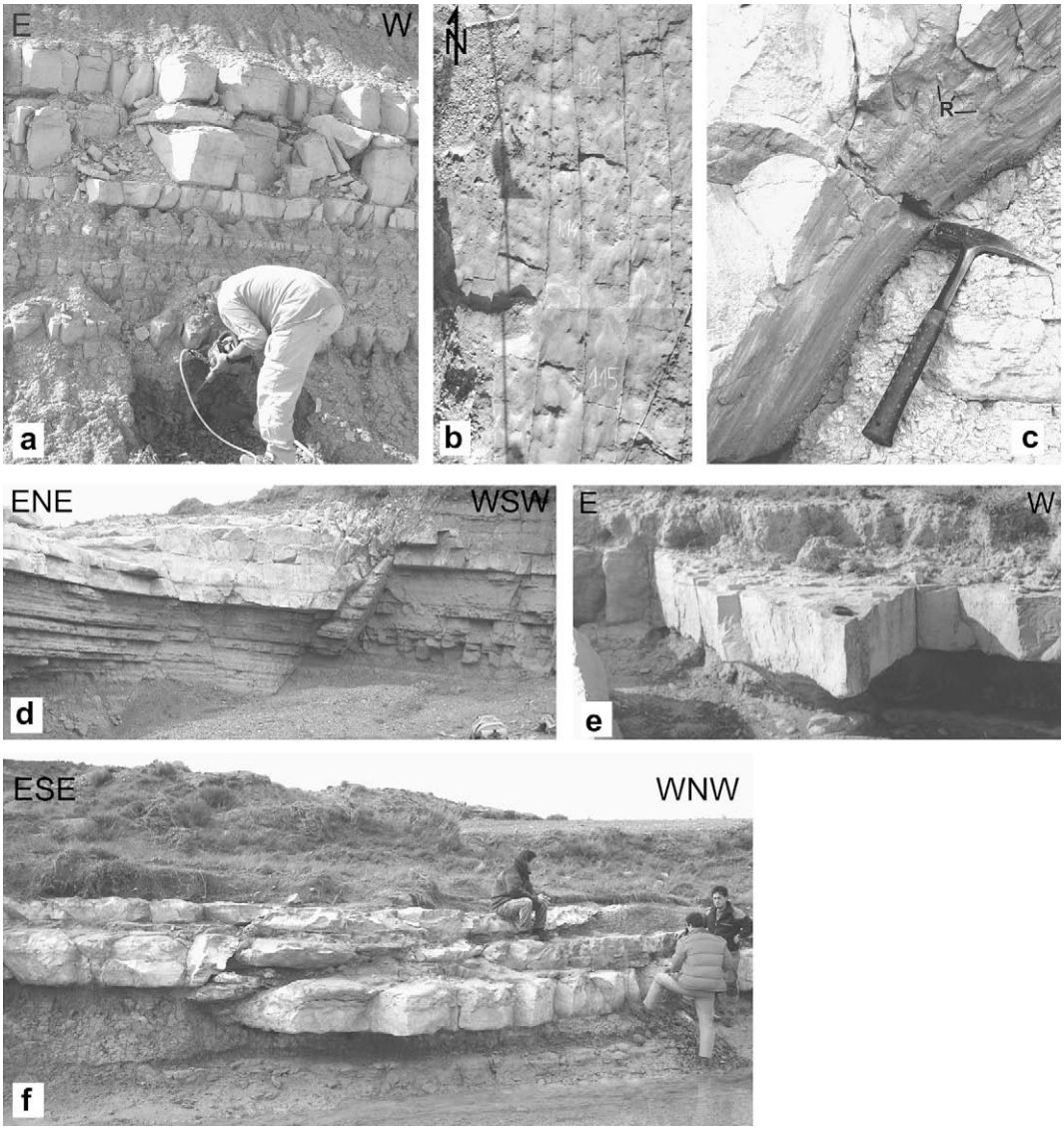

Fig. 2. Field examples of different types of faults and joints found in the central part of the Ebro basin. (a) N–S tensional joints at the Monegros area in an AMS site. (b) Plan-view of N–S and E–W tensional joints. (c) *Hydroplastic* fault at the Barranco de Tudela, in the Bardenas Reales sector. Note the curved, striated surfaces with Riedel steps R. (d) N–S striking normal faults. (e) N–S striking hybrid joints displaying a low dihedral angle. (f) E–W striking reverse fault at the Barranco de Tudela, in the Bardenas Reales sector.

strike-slip faults are often less than some tens of meters in length and show small displacements between few centimetres and 1 m (Fig. 2f). E–W striking reverse faults are scarce and, together with NNW to NNE trending strike-slip faults, are only found at the Bardenas Reales area. N–S striking joints are systematic and are ubiquitous throughout the central part of the Ebro basin (Fig. 2a). Most of these joints show either smooth surfaces or well-developed hackle marks and ribs that do not show shear indicators, and are interpreted as tensional joints. In other cases, these joints are arranged in low-dihedral conjugate pairs that display en echelon Riedel fractures and joint spectra, and are interpreted as hybrid (shear plus tensional) joints (Fig. 2e). N to NE striking normal faults (Fig. 2d) are also ubiquitous throughout the internal part of the Ebro basin, with N–S and NE–SW trending faults being predominant at the Bardenas Reales and Monegros areas, respectively. Finally, E–W trending joints correspond to tensional fractures that constitute the cross-joints of the N–S joint system (Fig. 2b).

Most of the studied faults and joints seem to have propagated in partially lithified sediments. No crystalline infill in veins, neither fault slickenfibres have been found in the numerous sampled sites. The only shear indicators observed on reverse, strike-slip and normal fault surfaces are synthetic Riedel secondary microfractures, which suggests a non-pure brittle behaviour of the deformed material. Finally, most faults have undulated surfaces without frictional polishing that show short, irregularly tapered grooves (Fig. 2c), which typically characterize *hydroplastic* faults (Petit and Laville, 1987).

At the map scale, the Bardenas Reales area presents a dense set of N–S to NE–SW striking normal faults, often shorter than 500 m in length, although they might reach down to 50 m and up to 2 km, and show measured displacements of up to 12 m (Fig. 2d). At the Monegros area, the dominant set of normal faults at the map scale strikes NW–SE to WNW–ESE and is expressed as a highly penetrative tectolineament system in satellite images and aerial photographs (Arlegui and Soriano, 1998). The main differences between the two selected areas are the absence of reverse and strike-slip faults in the Monegros sector and the different orientation of the normal faults found in the two areas.

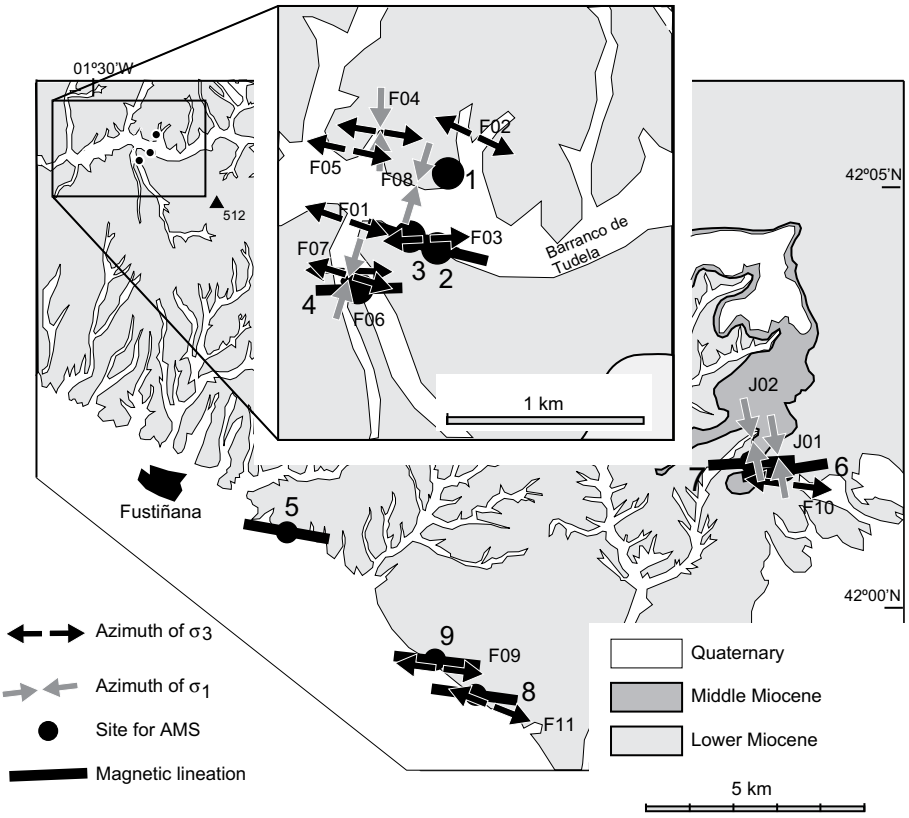

Fig. 3. Geological map of the Bardenas Reales area, with location of the studied sites. The inset shows a detailed view of the Barranco de Tudela.

These fault and joint systems have been studied with an ensemble of stress inversion methods (Arlegui, 1996; Arlegui and Simón, 1998, 2001; Simón et al., 1999) in order to establish the tectonic evolution of the Ebro foreland basin within the geodynamic scenario of the northeastern Iberian Peninsula. Striated fault populations were analysed with the Right Dihedra Method (a simple geometric–kinematic approach, Pegoraro, 1972; Angelier and Mechler, 1977), and the y-R Diagram (Simón Gómez, 1986) and Etchecopar (Etchecopar et al., 1981; Etchecopar, 1984) methods, which are based on the Bott equation (Bott, 1959). From the uppermost Cretaceous to the Late Miocene times, convergence between Europe, Iberia and Africa resulted in a N–S compression that evolved, in the course of the Late Miocene, to a WNW–ESE extension related to rifting at the eastern Iberian margin. As a result of this tectonic evolution, a sequence of coaxial stress systems developed. The N–S compression was characterized by a N–S trending σ_1 axis. Under this scenario, formation of E–W striking reverse faults and, later, of NNW to NNE striking strike-slip faults and N–S hybrid joints, indicates that the σ_3 axis evolved from a vertical to a horizontal position likely as a result of decrease of the horizontal N–S compressive stress. In the transition from N–S convergence to WNW–ESE extension, further decrease in the horizontal N–S compressive stress conditioned the switch of the σ_1 and σ_2 axes and the formation of N–S tensional joints under a small differential stress. The onset of WNW–ESE active extension led to increased differential stress and to formation of N–S normal faults (Arlegui and Simón, 1998, 2001; Simón et al., 1999). By late Neogene times, isostatic rebound at the Pyrenees probably reactivated NE–SW and NW–SE basement faults in the Monegros region, inducing the development of similarly oriented fractures in shallower stratigraphic levels. In the whole Ebro basin, where N–S striking joints were already present, they controlled the geometry and orientation of the new minor fractures formed orthogonally (i.e. secondary E–W tensional cross-joints) (Arlegui and Simón, 2001).

3. Materials and methods

In order to compare with the palaeostress data, we have sampled 14 sites in Lower and Middle Miocene lacustrine mudrocks that crop out at the central part of the Ebro basin (Fig. 1). Nine and five of these sites were collected at the Tudela and Alcubierre formations, which crop out extensively at the Bardenas Reales (Fig. 3) and Monegros (Fig. 4) areas, respectively. We have selected these two areas because they show considerable differences with regard to the presence and characteristics of the fracture systems. The Tudela and Alcubierre formations include, among other sediments, thick flat-lying lacustrine sequences of alternating white-greyish limestones and bluish-greyish mudrocks (Arenas and Pardo, 1999). Limestones were deposited in shallow lacustrine and palustrine environments, whereas bluish-greyish mudrocks formed in offshore lake areas (Arenas and Pardo, 1999). We have focused our sampling on lacustrine mudrocks from these formations because: 1) they are indicative of very low-energy environments, where the effect of paleocurrents and the content of ferromagnetic (*sensu lato*) minerals are minimised; 2) they had pores saturated with water at the time of deposition, which might have enabled particulate flow as a result of initial deformation; 3) they are flat-lying, therefore any fabric must have developed under the solely influence of layer-parallel compression or extension; 4) they are often related to limestones where palaeostress data can be obtained and compared to AMS results; 5) magnetostratigraphic results from the Tudela (Larrasoaña et al., 2006) and Alcubierre

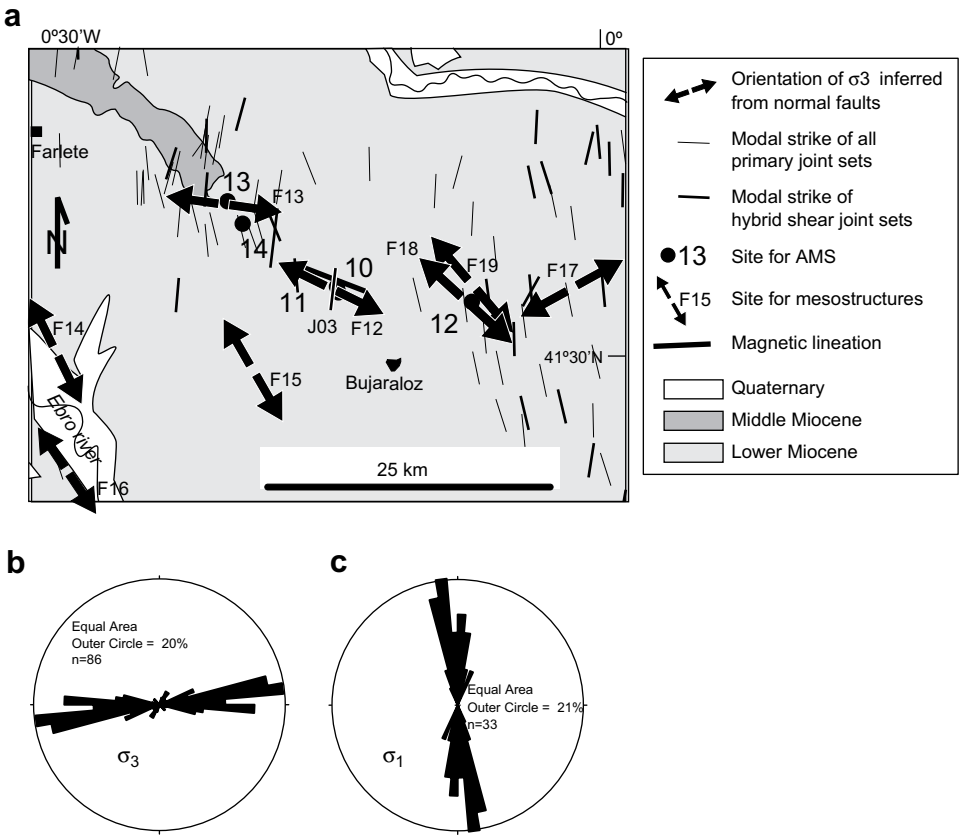

Fig. 4. (a) Geological map of the Monegros area, with location of the studied sites. (b) Rose diagram of σ_3 from all primary joints measured in the Monegros area. (c) Rose diagram of σ_1 only from hybrid shear joint sets.

(Pérez-Rivarés et al., 2002) formations provide accurate dating of all the sites, whose age range between the upper Early (ca. 19.4 Ma) and the lower Middle (ca. 16 Ma) Miocene. These magnetostratigraphic studies also indicate that the central sector of the Ebro basin is not affected by vertical-axis rotations that might disturb the original orientation of the magnetic fabric. All the sites collected from the Alcubierre Formation, together with 8 sites taken from the Tudela Formation, were drilled in thick mudrock intervals located away (>1 m) from limestone intercalations. Only one site from the Tudela Formation (site 1) is located within a thin (20 cm) mudrock interval sandwiched between two thick (>1.5 m) limestone beds in order to study the possible effect of this condition on deformation.

At every site, 7–10 cores were collected using a portable gas-powered drill. All the cores were sliced in standard paleomagnetic specimens. The low-field AMS of 14 or 15 specimens per site was measured using an AGICO KLY-2 susceptibility metre at the "Jaume Almera" Institute of Earth Sciences in Barcelona (Spain), following the scheme of Jelínek (1978). The AMS is a second-rank tensor that can be graphically displayed by a three-axes ellipsoid with a given orientation, shape and degree of anisotropy. Analysis of AMS data has been performed following the bootstrap method of Tauxe (1998). This method involves the calculation of the matrix elements and residual errors of each individual sample within a site, which are then used to obtain the orientation of the three principal eigenvectors ($k_{max} > k_{int} > k_{min}$) of the magnetic ellipsoid, together with their associated eigenvalues and confidence ellipses, at the site level. The shape and degree of anisotropy of the magnetic ellipsoids have been described using the T and Pj parameters of Jelínek (1981), respectively.

In order to constraint the relative contribution of paramagnetic and ferromagnetic *s.l.* minerals to the magnetic susceptibility, and to identify its mineralogical source, we have carried out hysteresis measurements and XRD analyses of representative samples. Hysteresis experiments were conducted using a Princeton Measurements Corporation Micromag 2900 vibrating sample magnetometer (VSM) at the National Oceanography Centre, Southampton (NOCS), UK, and XRD analyses were carried out at the "Jaume Almera" Institute using a Siemens D 501 diffractometer.

4. Results

4.1. Magnetic fabric

The magnetic susceptibility of the studied mudrocks ranges between 69 and 209 $\times 10^{-6}$ SI, although the majority of the specimens is in the range of 100–200 $\times 10^{-6}$ SI (Fig. 5a and Table 1). X-ray diffraction results indicate that the studied rocks are very homogeneous in composition (Fig. 5b), so that they conform to typical lacustrine mudrocks from the Ebro basin (see Arenas and Pardo, 1999). Calcite is the main mineral constituent and ranges between 30 and 60% in weight likely as a result of productivity in the lake system. Between ca. 22 and 35% of the mudrocks is constituted by the clay minerals illite and chlorite, which are interpreted to be detrital in origin in Tertiary sediments from the Ebro basin (Inglès et al., 1998). Quartz, which is also detrital, ranges between 7 and 17% in abundance. Other minor constituents are feldspars and carbonates such as dolomite and ankerite. The later appears only in some samples and its concentration rarely reaches more than a few percent (<6%) of the rock fraction. Ankerite is, therefore, unlikely to control the susceptibility signal of the studied mudrocks, whose behaviour is dominated by the paramagnets illite and chlorite as demonstrated by hysteresis experiments (Fig. 5c).

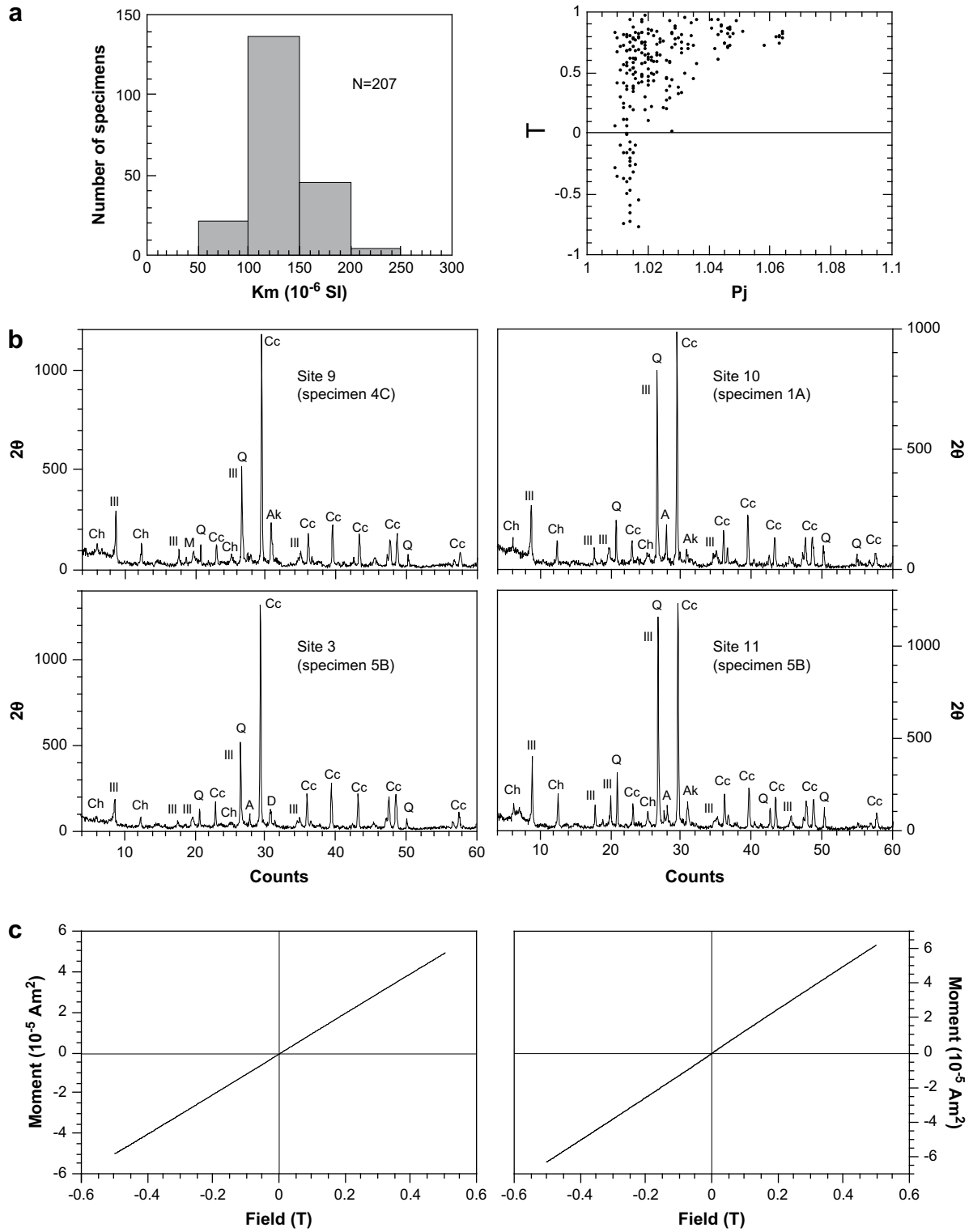

Fig. 5. (a) Frequency distribution of the mean susceptibility (k_m) values (left) and Pj–*T* plot (right) of all the studied specimens. (b) XRD results of representative mudrocks from the Bardenas Reales (left) and Monegros (right) areas. Cc: calcite; Q: quartz; Ill: illite; Ch: chlorite; A: albite; M: microcline; D: dolomite; Ak: ankerite. (c) Hysteresis results from two representative samples of Lower-Middle Miocene lacustrine mudrocks collected at the Bardenas Reales area.

Thus, a comparison between the high-field (at ca. 0.5 T) and the bulk magnetic susceptibility indicates that the paramagnetic fraction represents more than 90% of the measured magnetic susceptibilities. Overall, these results indicate that the magnetic fabric of the studied rocks results from the preferred orientation of phyllosilicate (illite and chlorite) grains.

All the studied sites have Pj and *T* values typical for weakly deformed mudrocks (Fig. 5a and Table 1). Pj values of individual specimens range between 1.01 and 1.06. *T* values usually range between 0.5 and 1, although negative *T* values as low as ca. −0.7 are also found. Site-mean Pj values are always lower than 1.028 at the Bardenas Reales, and range between 1.017 and 1.054 at the

Table 1
Summary of magnetic anisotropy results computed for each site.

Site	N	k_m	std	Pj	std	T	std	k_{max}				k_{int}			K_{min}			Magnetic ellipsoid Type
								τ_1	D	I	ε_{1-2}	τ_2	D	I	τ_3	D	I	
Bardenas Reales area																		
1	14	128.9	10.1	1.018	0.005	0.722	0.110	0.3351	169.1	3.9	90.0	0.3348	78.6	7.3	0.3301	286.8	81.7	1
2	15	96.5	6.4	1.013	0.002	−0.114	0.186	0.3354	102.6	3.4	10.4	0.3332	12.5	1.9	0.3313	253.8	86.1	4
3	15	124.2	22.3	1.014	0.002	−0.451	0.211	0.3357	288.3	0.6	8.1	0.3326	198.3	1.5	0.3317	41.0	88.3	3
4	15	121.5	5.8	1.016	0.003	0.556	0.164	0.3352	268.0	4.6	25.6	0.3344	176.7	15.2	0.3304	14.4	74.1	2
5	15	124.9	3.5	1.028	0.003	0.340	0.127	0.3373	100.0	2.4	7.2	0.3344	9.9	2.2	0.3284	237.8	86.7	3
6	15	123.7	7.9	1.013	0.002	0.639	0.137	0.3348	261.4	0.2	20.6	0.3342	351.5	13.9	0.3310	170.8	76.1	2
7	14	98.2	19.6	1.015	0.003	0.641	0.191	0.3350	86.4	9.1	29.7	0.3344	177.3	5.4	0.3306	297.4	79.4	2
8	15	163.0	20.5	1.017	0.004	0.489	0.300	0.3354	97.8	9.0	22.1	0.3343	188.0	0.9	0.3303	283.5	81.0	2
9	14	155.8	18.7	1.021	0.003	0.526	0.267	0.3359	96.6	5.3	16.5	0.3345	187.0	4.0	0.3296	314.0	83.3	2
Monegros area																		
10	15	148.4	5.8	1.017	0.003	0.563	0.177	0.3354	111.6	3.6	17.8	0.3344	202.0	6.5	0.3302	353.1	82.6	2
11	15	188.2	20.1	1.054	0.010	0.789	0.083	0.3390	63.0	7.7	36.2	0.3376	332.8	1.1	0.3234	234.7	82.2	1
12	15	115.9	6.9	1.045	0.002	0.810	0.094	0.3379	99.2	0.1	41.5	0.3371	189.2	4.7	0.3251	8.1	85.3	1
13	15	114.3	10.0	1.031	0.005	0.772	0.109	0.3365	337.8	2.1	49.9	0.3360	67.9	3.1	0.3275	213.5	86.2	1
14	15	140.3	31.3	1.025	0.006	0.791	0.084	0.3359	83.8	0.8	73.5	0.3355	173.8	5.3	0.3286	345.7	84.6	1

N = number of specimens. $k_m = (k_{max} + k_{int} + k_{min})/3$ (mean susceptibility. in 10^{-6} SI units). $Pj = \exp\{2[(\eta_1 - \eta)^2 + (\eta_2 - \eta)^2 + (\eta_3 - \eta)^2]\}^{1/2}$ (Jelínek, 1981). $T = [2(\eta_2 - \eta_3)/(\eta_1 - \eta_3)] - 1$ (shape factor; Jelínek, 1981). std = standard deviation of the previous column value. D, I = Declination and inclination. τ_1, τ_2, τ_3 = Eigenvalues of tensor representing k_{max}, k_{int} and k_{min}, respectively (Tauxe, 1998). ε_{1-2} = semi-angle of the confidence ellipse around k_{max} from Tauxe's statistics (Tauxe, 1998).

Monegros area (Table 1). Site-mean T values range between 0.3 and 0.7 at seven of the studied sites, and are larger and lower than 0.7 and −0.1 at five and two sites, respectively. These results indicate weak fabrics that range between clearly oblate ($T > 0.7$), oblate to triaxial ($0.3 < T > 0.7$) and prolate ($T < -0.1$) in shape.

The magnetic fabric of the studied mudrocks can be grouped into four types of magnetic ellipsoids according to their directional properties (Fig. 6):

- Type 1 is characterized by a tight clustering of k_{min} around the bedding pole and also by a large dispersion of k_{max} and k_{int} throughout the bedding plane. According to this scattering, the semi-angle (ε_{12}) of the confidence ellipse around the k_{max} axes in the k_{max}–k_{int} plane is largest (>30°). The histograms of bootstrapped eigenvalues indicate that k_{max} and k_{int} have similar values and cannot be statistically distinguished from each other (Fig. 6c). According to these results, no magnetic lineation defined by the site-mean orientation of k_{max} axes can be statistically distinguished at these sites.
- Type 2 is also characterized by a tight clustering of k_{min} around the bedding pole; k_{max} and k_{int} are also scattered throughout the bedding plane, although their grouping is slightly improved with respect to Type 1 as indicated by smaller ε_{12} values ($15° < \varepsilon_{12} < 30°$). The histograms of bootstrapped eigenvalues indicate that k_{max} and k_{min} are statistically distinctive from each other despite of having similar values. This indicates that, although weak, a magnetic lineation can be distinguished in these sites.
- In Type 3, k_{min} remains tightly clustered around the bedding pole and k_{max} and k_{int} appear well grouped at near 90° away from each other. Accordingly, ε_{12} values are smaller (<15°) and their bootstrapped eigenvalues are clearly distinctive, demonstrating the presence of a well-defined magnetic lineation.
- Type 4 is also characterized by a well-defined lineation ($\varepsilon_{12} < 15°$). The only difference with respect to Type 3 concerns the distribution of k_{min} axes, which are scattered forming a girdle perpendicular to k_{max}.

Among all the studied sites, only one from the Bardenas Reales and four from the Monegros have magnetic fabric of Type 1. As expected, the site-mean directions of k_{max} at these sites do not show a systematic trend (Table 1). The remaining site from the Monegros area (site 10), and all but one site from the Bardenas Reales (site 1), can be included into Type 2 (6 sites), Type 3 (2 sites) and Type 4 (1 site) fabrics (Table 1). In all these cases, the magnetic lineations show a systematic near E–W direction.

4.2. AMS vs. palaeostress results

In this section we compare the orientation of AMS axes with palaeostress results obtained nearby the AMS sites. With the exception of site 1, AMS sites at the Bardenas Reales area (Fig. 3) have their k_{max} axes oriented 098 on average (Table 1), exactly perpendicular to the orientation of σ_1 axes (average 008) determined from strike-slip fault populations (Table 2). Noticeably, k_{max} axes are also strikingly similar to the orientation of σ_3 axes (average 101) determined from normal fault populations (Table 2). Table 3 shows a comparison between the trends of k_{max} axes of individual AMS sites and σ_1 (from compressive structures) and σ_3 (from extensional structures) axes determined in the nearest site(s) of brittle mesostructures. The angle between σ_1 and the perpendicular to k_{max} varies between 1.4° and 16.6°. This angle is always smaller than the corresponding ε_{12} angle, which indicates that the magnetic and the compressive palaeostress ellipsoids are virtually coaxial in all cases (Table 3). The angle between σ_3 and k_{max} ranges between 3° and 23.3°, and in two cases is larger than the corresponding ε_{12} angle. This indicates that the magnetic and the extensional palaeostress ellipsoids are not always coaxial.

5. Discussion

5.1. Origin of the magnetic lineation

The magnetic fabric from the Ebro basin is very similar to those described for other weakly deformed mudrocks undergoing incipient tectonic deformation (Borradaile and Tarling, 1981; Kissel et al., 1986; Averbuch et al., 1992; Parés and Dinarès-Turell, 1993; Sagnotti and Speranza, 1993; Mattei et al., 1995, 1997; Sagnotti et al., 1998, 1999; Parés et al., 1999; Cifelli et al., 2004a,b; Larrasoaña et al., 2004). Type 1 ellipsoids described here correspond to the "undeformed state" (see Parés, 2004), in which an oblate (e.g. sedimentary) magnetic fabric results from the deposition of platy phyllosilicates parallel to the water–sediment interface and randomly-oriented throughout this surface, as well as from subsequent compaction driven by overburden pressure (Sintubin, 1994). The remaining magnetic ellipsoids described here are

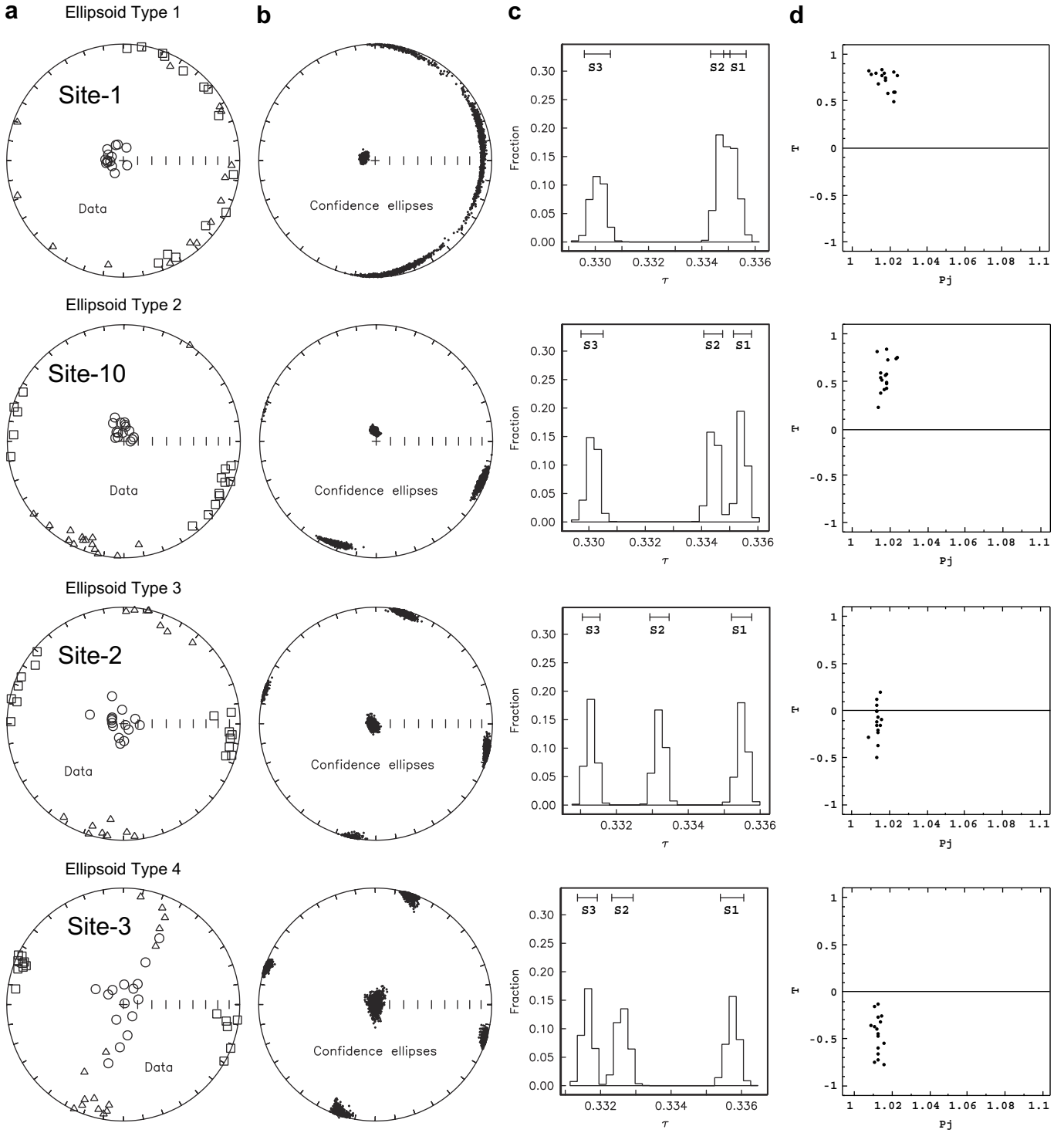

Fig. 6. Examples showing the four typical magnetic ellipsoids found in the studied area. (a) Equal area, lower hemisphere projection of the maximum (squares), intermediate (triangles) and minimum (circles) susceptibility axes (eigenvectors). (b) Equal area, lower hemisphere projection of the bootstrapped eigenvectors. (c) Histogram showing Cartesian coordinates S1, S2 and S3 of the bootstrapped eigenvectors. (d) Pj–*T* plot with all specimens from the site.

included within the "earliest deformation stage" (Parés, 2004), when incipient deformation drives rotation of platy phyllosilicates within the bedding plane so that their long axes become progressively aligned perpendicular to the shortening direction. This results in initial development of a weak, yet statistically significant, magnetic lineation (Type 2 ellipsoids) that becomes progressively enhanced till the magnetic ellipsoid changes from oblate to triaxial (Type 3 ellipsoids) and then to prolate (Type 4 ellipsoids) in shape.

Magnetic ellipsoids represent material tensors, whereas palaeostress ellipsoids are ephemeral field tensors. Thus, for magnetic fabric to be reliable indicator of palaeostress directions it must be blocked at a brief time span during or shortly after deposition (e.g. Larrasoaña et al., 2004), so that it represents an incremental strain ellipsoid. Two pieces of evidence support the hypothesis that both the compressive and the extensional stress fields considered in this work acted during or shortly after

Table 2
List of palaeostress results obtained at sites with available magnetic anisotropy data.

Site	Explained structures/total	Kind of tensor	Trend of σ_1	Trend of σ_2	Stress ratio Re	Data source
Faults						
Bardenas Reales sector						
F-01	37/47	Extension	Vertical	110	0.42	a
F-02	6/6	Extension	Vertical	099	0.69	b
F-03	63/80	Extension	Vertical	085	0.23	c
F-04	11/52	Strike slip	002	092	0.06	b
	33/52	Extension	Vertical	101	0.23	
F-05	12/14	Extension	Vertical	103	0.10	a,b
F-06	28/256	Strike slip	013	102	0.28	c
	137/256	Extension	Vertical	092	0.19	
F-07	34/56	Extension	Vertical	108	0.48	b
F-08	62/80	Strike slip	011	112	0.02	c
F-09	13/15	Extension	Vertical	103	0.28	b
F-10	16/18	Extension	Vertical	101	0.24	c
Monegros sector						
F-11	37/52	Extension	Vertical	112	0.22	c
F-12	21/23	Extension	Vertical	116	0.02	b
F-13	8/8	Extension	Vertical	097	0.24	b
F-14	25/28	Extension	Vertical	148	0.07	b
F-15	19/20	Extension	Vertical	149	0.07	b
F-16	18/20	Extension	Vertical	146	0.02	b
F-17	17/18	Extension	Vertical	061	0.04	b
F-18	12/12	Extension	Vertical	132	0.00	b
F-19	13/13	Extension	Vertical	139	0.00	b
Hybrid joints						
Bardenas Reales sector						
J-01	34/34	Strike slip	170	080	–	d
J-02	36/36	Strike slip	168	078	–	d
Monegros sector						
J-03	31/31	Strike slip	005	095	–	d

Stress ratio Re (shape of the stress ellipsoid parameter) = $(\sigma_2 - \sigma_3)/(\sigma_1 - \sigma_3)$. Data source: a: Simón et al. (1999); b: Arlegui and Simón (1998); c: previously unpublished data; d: new data.

sedimentation of the studied materials, Early to Middle Miocene in age. First, they represent regional stress fields whose activity in NE Iberia by that time is widely documented. The N–S, Pyrenean compression produced contractional structures in the Ebro basin (Arlegui and Simón, 1998, 2001; Simón et al., 1999), Pyrenees (e.g. Muñoz, 1992) and Iberian ranges (e.g. Muñoz-Jiménez and Casas-Sainz, 1997; Capote et al., 2002; Simón, 2006). The E–W to ESE–WNW extension, driven by rifting at the Valencia Through, gave rise to the onshore extensional grabens of Teruel and Maestrat (e.g. Vegas et al., 1979; Simón, 1982; Anadón and Moissenet, 1996). Second, most of the studied fractures propagated in partially lithified sediments (e.g. *hydroplastic* faults). In consequence, blocking of the magnetic fabric under the same stress conditions that produced the analysed faults constitutes the most realistic scenario, and other alternative hypothesis such as modification of the fabric by later fault activity after consolidation can be rejected.

Several studies have suggested that magnetic lineations can develop either perpendicular to the contemporary σ_1 axis in compressive settings (Kissel et al., 1986; Lee et al., 1990; Mattei et al., 1997; Sagnotti et al., 1999) or parallel to the σ_3 axis in extensional contexts (Sagnotti et al., 1994; Mattei et al., 1999; Cifelli et al., 2004a, 2005; Borradaile and Hamilton, 2004; Soto et al., 2007). Among the two feasible stress regimes considered for the development of our magnetic fabric, a compressive origin is supported by the following observations. First, two sites with the better-developed lineation (i.e. lowest *T* values, Table 1) are sites 2 and 3, which are located on the hanging-wall and footwall, respectively, of a small reverse fault at the Bardenas Reales area (Fig. 2f). Second, all but one of the sites with a statistically-significant magnetic lineation are located in the Bardenas Reales, where compressive structures are better developed than in the Monegros area. This difference might be attributed to a shorter distance of the

Table 3
Comparison of palaeostress and magnetic anisotropy results.

AMS			σ_1 from compressional structures				σ_3 from extensional structures			
Site	Trend k_{max} (0–180°)	ε_{12}	Site	Distance (m)	Trend of σ_1	Angle ($k_{max} - 90°$) – σ_1	Site	Distance (m)	Trend of σ_3	Angle ($k_{max} - \sigma_3$)
Bardenas Reales sector										
2	103.6	10.4	F-08	~50 m	011	2.6	F-03	<50 m	085	18.6[a]
3	108.3	8.1	F-08	~350 m	011	7.3	F-03	<50 m	085	23.3[a]
4	088	25.6	F-06	<50 m	013	15	F-06	<50 m	092	4
5	100	7.2					F-09	~4.5 km	103	3
6	081.4	20.6	J-01	~250 m	170	1.4	F-10	<50 m	101	19.6
7	086.4	29.7	J-02	~750 m	168	8.4	F-10	~1 km	101	14.6
8	097.8	22.1					F-11	<50 m	112	14.2
9	096.6	16.5					F-09	<50 m	103	6.4
Monegros sector										
10	111.6	17.8	J-03	~500 m	005	16.6	F-12	<50 m	116	4.4

[a] Sites with the angle between k_{max} and σ_3 higher than the corresponding ε_{12} angle.

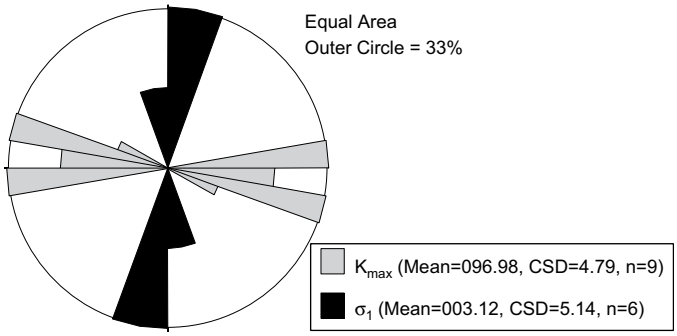

Fig. 7. Rose diagram of k_{max} of all sites with magnetic ellipsoids of Types 2, 3 and 4 (data from Table 1) and σ_1 only from compressive structures (data from Table 2). CSD: Circular standard deviation.

Bardenas Reales area to the Pyrenees, whence the compressive stress field is supposed to have propagated. Finally, the magnetic lineation is always coaxial with the synsedimentary N–S compression but not with the subsequent WNW–ESE extension (Table 3).

5.2. Reliability of the magnetic fabric as palaeostress indicator in compressive settings

Up to date, few studies have shown that the magnetic lineation is perpendicular to the maximum stress axis (σ_1) in compressive settings (Kissel et al., 1986; Lee et al., 1990; Mattei et al., 1997; Sagnotti et al., 1999). Our results show that the angle between σ_1 and the perpendicular to the magnetic lineation varies between 1.4° and 16.6°, which is always smaller than the corresponding ε_{12} angle at the site scale (Table 3). This implies that the magnetic lineation and the σ_1 axis are systematically perpendicular within the ε_{12} error associated to k_{max}, demonstrating that the magnetic lineation of weakly deformed rocks can be used as a paleostress indicator in compressive settings. It is important to note that, in order to use magnetic fabric to determine regional paleostress directions, a regional study is needed to avoid possible anomalies or local stress deflections. A comparison between all the magnetic fabric with a statistically-significant magnetic lineation (i.e. Type 2, 3 and 4 ellipsoids) with paleostress results from the Ebro basin demonstrates that the magnetic lineation is perpendicular to σ_1 at a regional scale (Fig. 7), which further supports the reliability of magnetic fabric.

The use of magnetic fabric of weakly deformed mudrocks as a paleostress indicator has not only some advantages against brittle mesostructural analysis, but also some shortcomings that need to be considered. Magnetic fabric of weakly deformed mudrocks is blocked during the earliest diagenesis and remains locked during subsequent deformation (e.g. Parés et al., 1999; Parés, 2004; Larrasoaña et al., 2004), thereby recording the prevailing stress conditions during a short period (i.e. after the deposition and before the consolidation of the material). On the contrary, the analysis of brittle mesostructures records the prevailing stress conditions over longer time spans, from the consolidation of the material onwards (Soto et al., 2007). Therefore, magnetic fabric enables a more straightforward interpretation compared with brittle mesostructure analysis, since overprinting of different fracture systems (sometimes showing complex time relationships) could make it difficult to discern successive stress systems. However, for magnetic fabric to be a reliable paleostress indicator, the following limitations need to be considered. Magnetic fabric must be analysed in materials where the possible effect of paleocurrents is minimised and the paramagnetic minerals represent the major contributors to the bulk susceptibility. These conditions are satisfied by mudrocks deposited under sub-aquatic conditions (i.e. lacustrine or marine), where the sediments are saturated in water enabling particulate flow as a result of incipient deformation. Coarse sandstones or rocks with high quantities of ferromagnetic minerals *s.l.* must be avoided. In addition, thin stratigraphic intervals sandwiched between rheologically stronger beds (e.g. mudrocks between limestones beds) must be avoided also because deformation is likely accommodated by fractures developed on the stronger beds. This is the case of site 1 located at the Bardenas Reales area, which was taken from a 20-cm thick mudrock interval sandwiched between two thick limestone beds. This site has the highest ε_{12} angle (i.e. pure sedimentary fabric) despite of being located near compressive structures (Fig. 3) and AMS sites with a well-developed lineation.

6. Conclusions

This work demonstrates the validity of using AMS as a palaeostress indicator in compressive settings in weakly deformed mudrocks. The foreland Ebro basin was chosen to compare both methodologies due to the good knowledge of its Neogene stress field evolution and the presence of suitable outcrops both for AMS and for palaeostress analyses. The AMS data collected in weakly deformed mudrocks, Early to Middle Miocene in age, define a compactional (sedimentary) magnetic foliation at all sites. In 9 of these sites, a well-defined magnetic lineation oriented E–W attests for a subtle tectonic overprint. This is related to N–S compression linked to the convergence between Europe, Iberia and Africa. The magnetic and the palaeostress ellipsoids are coaxial both at local and at regional scales, thereby validating the reliability of AMS as a palaeostress indicator in compressional settings in weakly deformed mudrocks.

Acknowledgements

This work was supported by the project CGL2006-09670/BTE of the Dirección General de Enseñanza Superior (DGES), Spanish Ministry of Science and FEDER. Financial support was also given by two research contracts, JAE-Doc (CSIC) and "Ramón y Cajal" Programs (Spanish Ministry of Science) for R.S and J.C.L, respectively. We are grateful to T. Debacker and an anonymous reviewer, who helped to substantially improve the first version of the manuscript, and R.E. Holdsworth for his helpful editorial handling.

References

Alonso-Zarza, A.M., Armenteros, A., Braga, J.C., Muñoz, A., Pujalte, V., Ramos, E., Aguirre, J., Alonso-Gavilán, G., Arenas, C., Baceta, J.I., Carballeira, J., Calvo, J.P., Corrochano, A., Fornós, J.J., González, A., Luzón, A., Martín, J.M., Pardo, G., Payros, A., Pérez, A., Pomar, L., Rodríguez, J.M., Villena, J., 2002. Tertiary. In: Gibbons, W., Moreno, T. (Eds.), The Geology of Spain, Geological Society, London, pp. 293–334.

Anadón, P., Moissenet, E., 1996. Neogene basins in the Eastern Iberian range. In: Friend, P.F., Dabrio, C.J. (Eds.), Tertiary Basins of Spain: The Stratigraphic Record of Crustal Kinematics. Cambridge Univ. Press, Cambridge, pp. 68–76.

Angelier, J., Mechler, P., 1977. Sur une méthode graphique de recherche des contraintes principales également utilisable en tectonique et en séismologie: la méthode des dièdres droits. Bulletin de la Société Géologique de France 19 (7), 1309–1318.

Arenas, C., Pardo, G., 1999. Latest Oligocene-late Miocene lacustrine systems of the north-central part of the Ebro Basin (Spain): sedimentary facies model and paleogeographic synthesis. Palaeogeography, Palaeoclimatology, Palaeoecology 151, 127–148.

Arlegui, L.E., 1996. Diaclasas, fallas y campo de esfuerzos en el sector central de la Cuenca del Ebro. Ph.D. Thesis. University of Zaragoza, 308 pp.

Arlegui, L.E., Simón, J.L., 1998. Reliability of palaeostress analysis from fault striations in near multidirectional extension stress fields: example from the Ebro Basin, Spain. Journal of Structural Geology 20, 827–840.

Arlegui, L.E., Simón, J.L., 2001. Geometry and distribution of regional joint sets in a non-homogeneous stress field: case study in the Ebro basin (Spain). Journal of Structural Geology 23, 297–313.
Arlegui, L.E., Soriano, M.A., 1998. Characterising lineaments from satellite images and field studies in the central Ebro basin (NE Spain). International Journal of Remote Sensing 19, 3169–3185.
Averbuch, O., Frizon de Lamotte, D., Kissel, C., 1992. Magnetic fabric as a structural indicator of the deformation path within a fold-thrust structure: a test case from the Corbieres (NE Pyrenees, France). Journal of Structural Geology 14, 461–474.
Benn, D.I., 1994. Fabric shape and the interpretation of sedimentary fabric data. Journal of Sedimentary Research A64 (4), 910–915.
Borradaile, G.J., Tarling, D.H., 1981. The influence of deformation mechanism in magnetic fabrics of weakly deformed rocks. Tectonophysics 77, 151–168.
Borradaile, G.J., Henry, B., 1997. Tectonic applications of magnetic susceptibility and its anisotropy. Earth-Science Reviews 42, 49–93.
Borradaile, G.J., Hamilton, T., 2004. Magnetic fabrics may proxy as neotectonic stress trajectories, Polis rift, Cyprus. Tectonics 23, TC1001, doi:10.1029/2002TC001434.
Bott, M.H.P., 1959. The mechanics of oblique slip faulting. Geological Magazine 96, 109–117.
Capote, R., Muñoz, J.A., Simón, J.L., Liesa, C.L., Arlegui, L.E., 2002. Alpine tectonics I: the Alpine system north of the Betic Cordillera. In: Gibbons, W., Moreno, T. (Eds.), The Geology of Spain, Geological Society, London, pp. 385–397.
Cifelli, F., Rosetti, F., Mattei, M., Hirt, A.M., Funiciello, R., Tortorici, L., 2004a. An AMS, structural and paleomagnetic study of quaternary deformation in eastern Sicily. Journal of Structural Geology 26, 29–46.
Cifelli, F., Mattei, M., Hirt, A.M., Gunther, A., 2004b. The origin of tectonic fabrics in "undeformed" clays: the early stages of deformation in extensional sedimentary basins. Geophysical Research Letters 31, L09604, doi:10.1029/2004GL019609.
Cifelli, F., Mattei, M., Chadima, M., Hirt, A.M., Hansen, A., 2005. The origin of tectonic lineations in extensional basins: Combined neutron texture and magnetic analyses of "undeformed" clays. Earth and Planetary Science Letters 235, 62–78.
Etchecopar, A., 1984. Etude des états de contraintes en tectonique cassante et simulations de déformations plastiques (approche matématique). Unpublished Ph.D. Thesis. USTL Montpellier.
Etchecopar, A., Vasseur, G., Daignieres, M., 1981. An inverse problem in microtectonics for the determination of stress tensors from fault striation analysis. Journal of Structural Geology 3, 51–65.
García-Castellanos, D., Vergés, J., Gaspar-Escribano, J., Cloetingh, S., 2003. Interplay between tectonics, climate and fluvial transport during the Cenozoic evolution of the Ebro basin (NE Iberia). Journal of Geophysical Research 108, 2357, doi:10.1029/2002JB002073.
Inglès, M., Salvany, J.M., Muñoz, A., Pérez, A., 1998. Relationship of mineralogy to depositional environments in the non-marine tertiary mudstones of the southwestern Ebro Basin (Spain). Sedimentary Geology 116, 159–176.
Jelínek, V., 1978. Statistical processing of anisotropy of magnetic susceptibility measured on groups of specimens and its applications. Studia Geophysica et Geodaetica 22, 50–62.
Jelínek, V., 1981. Characterization of the magnetic fabrics of rocks. Tectonophysics 79, 63–67.
Kissel, C., Barrier, E., Laj, C., Lee, T.Q., 1986. Magnetic fabric of "undeformed" marine clays from compressive zones. Tectonophysics 40, 287–308.
Larrasoaña, J.C., Pueyo, E.L., Parés, J.M., 2004. An integrated AMS, structural, palaeo- and rock-magnetic study of Eocene marine marls from the Jaca-Pamplona basin (Pyrenees, N Spain); new insights into the timing of magnetic fabric acquisition in weakly deformed mudrocks. In: Martín-Hernández, F., Lüneburg, C.M., Aubourg, C., Jackson, M. (Eds.), Magnetic Fabric: Methods and Applications. Geological Society, London, Special Publication, vol. 238, pp. 127–143.
Larrasoaña, J.C., Murelaga, X., Garcés, M., 2006. Magnetobiochronology of Lower Miocene (Ramblian) continental sediments from the Tudela Formation (western Ebro basin, Spain). Earth and Planetary Science Letters 243, 409–423.
Lee, T., Kissel, C., Laj, C., Horng, C.S., Lue, Y.T., 1990. Magnetic fabric analysis of the Plio-Pleistocene sedimentary formations of the Coastal Range of Taiwan. Earth and Planetary Science Letters 98, 23–32.
Mattei, M., Funiciello, R., Kissel, C., 1995. Paleomagnetic and structural evidence for Neogene block rotations in the Central Apennines, Italy. Journal of Geophysical Research 100, 17863–17883.
Mattei, M., Sagnotti, L., Faccenna, C., Funiciello, R., 1997. Magnetic fabric of weakly deformed clayey sediments in the Italian peninsula: relationships with compressive and extensional tectonics. Tectonophysics 271, 107–122.
Mattei, M., Speranza, F., Argentieri, A., Rosetti, F., Sagnotti, L., Funiciello, R., 1999. Extensional tectonics in the Amantea basin (Calabria, Italy): a comparison between structural and magnetic anisotropy data. Tectonophysics 307, 33–49.
Muñoz, J.A., 1992. Evolution of a continental collision belt: ECORS-Pyrenees crustal balanced cross-section. In: McClay, K.R. (Ed.), Thrust Tectonics. Chapman & Hall, London, pp. 235–246.
Muñoz-Jiménez, A., Casas-Sainz, A.M., 1997. The Rioja Trough (N Spain): tectosedimentary evolution of a symmetric foreland basin. Basin Research 9, 65–85.
Parés, J.M., 2004. How deformed are weakly deformed mudrocks? Insights from magnetic anisotropy. In: Martín-Hernández, F., Lüneburg, C.M., Aubourg, C., Jackson, M. (Eds.), Magnetic Fabric: Methods and Applications. Geological Society, London, Special Publication, vol. 238, pp. 191–203.
Parés, J.M., Dinarès-Turell, J., 1993. Magnetic fabric in two sedimentary rock types from the Southern Pyrenees. Journal of Geomagnetism and Geoelectricity 45, 193–205.
Parés, J.M., van der Pluijm, B.A., 2002. Evaluating magnetic lineations (AMS) in deformed rocks. Tectonophysics 350, 283–298.
Parés, J.M., van der Pluijm, B.A., Dinarés-Turell, J., 1999. Evolution of magnetic fabrics during incipient deformation of mudrocks (Pyrenees, Northern Spain). Tectonophysics 307, 1–14.
Pegoraro, O., 1972. Application de la microtectonique à un étude de neotectonique. Le golfe Maliaque (Grèce centrale). Unpublished Ph.D. Thesis, USTL Montpellier.
Pérez-Rivarés, F.J., Garcés, M., Arenas, C., Pardo, G., 2002. Magnetocronología de la sucesión miocena de la Sierra de Alcubierre (sector central de la Cuenca del Ebro). Revista de la Sociedad Geológica de España 15, 210–225.
Petit, J.P., Laville, E., 1987. Morphology and microstructures of hydroplastic slickensides in sandstone. In: Jones, M.E., Preston, R.M.F. (Eds.), Deformation of Sediments and Sedimentary Rocks. Geological Society Special Publication, vol. 29, pp. 107–112.
Richter, C., van der Pluijm, B.A., Housen, B., 1993. The quantification of crystallographic preferred orientation using magnetic anisotropy. Journal of Structural Geology 15, 113–116.
Sagnotti, L., Speranza, F., 1993. Magnetic fabric analysis of the Plio-Pleistocene clayey units of the Sant'Arcangelo basin, southern Italy. Physics of the Earth and Planetary Interiors 77, 165–176.
Sagnotti, L., Faccenna, C., Funiciello, R., Mattei, M., 1994. Magnetic fabric and structural setting of Plio-Pleistocene clayey units in an extensional regime: the Tyrrhenian margin of central Italy. Journal of Structural Geology 16, 1243–1257.
Sagnotti, L., Speranza, F., Winkler, A., Mattei, M., Funiciello, R., 1998. Magnetic fabric of clay sediments from the external northern Apennines (Italy). Physics of the Earth and Planetary Interiors 105, 73–93.
Sagnotti, L., Winkler, A., Montone, P., Di Bella, L., Florindo, F., Mariucci, M.T., Marra, F., Alfonsi, L., Frepoli, A., 1999. Magnetic anisotropy of Plio-Pleistocene sediments from the Adriatic margin of the northern Apennines (Italy): implications for the time-space evolution of the stress field. Tectonophysics 311, 139–153.
Simón, J.L., 1982. Compresión y distensión alpinas en la Cadena Ibérica oriental. Ph.D. Thesis. University of Zaragoza, Publ. Instituto de Estudios Turolenses (1984), 269 pp.
Simón Gómez, J.L., 1986. Analysis of a gradual change in stress regime (example from the eastern Iberian Chain, Spain). Tectonophysics 124, 37–53.
Simón, J.L., 2006. El registro de la compresión intraplaca en los conglomerados de la cuenca terciaria de Aliaga (Teruel, Cordillera Ibérica). Revista de la Sociedad Geológica de España 19, 163–179.
Simón, J.L., Arlegui, L.E., Liesa, C.L., Maestro, A., 1999. Stress perturbations registered by jointing near strike-slip, normal, and reverse faults: examples from the Ebro Basin, Spain. Journal of Geophysical Research 104, 15141–15153.
Sintubin, M., 1994. Clay fabrics in relation to the burial history of shales. Sedimentology 41, 1161–1169.
Soto, R., Casas-Sainz, A.M., Villalaín, J.J., Oliva-Urcia, B., 2007. Mesozoic extension in the Basque–Cantabrian basin (N Spain): contributions from AMS and brittle mesostructures. Tectonophysics 445 (3–4), 373–394, doi:10.1016/j.tecto.2007.09.007.
Tarling, D.H., Hrouda, F., 1993. The Magnetic Anisotropy of Rocks. Chapman & Hall, London, 217 pp.
Tauxe, L., 1998. Paleomagnetic Principles and Practice. Kluwer Academic Publishers, Dordrecht, 299 pp.
Vegas, R., Fontboté, J.M., Banda, E., 1979. Widespread neogene rifting superimposed on alpine regions of the Iberian Peninsula. Proceedings of the Symposium Evolution and Tectonics of the Western Mediterranean and Surrounding Areas, EGS, Viena. Instituto Geográfico Nacional Spec, Publ. 201, pp. 109–128.